JOURNAL OF MATERIALS SCIENCE 26 (1991) 4461–4467

Diffusional cubic-to-tetragonal phase transformation and microstructural evolution in ZrO_2–Y_2O_3 ceramics

Y. ZHOU, Q. L. GE, T. C. LEI
Department of Metals and Technology, Harbin Institute of Technology, Harbin 150006, People's Republic of China

T. SAKUMA
Department of Materials Science, Faculty of Engineering, University of Tokyo, Tokyo 113, Japan

The diffusional cubic-to-tetragonal (c–t) phase transformation and microstructural evolution were studied on ZrO_2–Y_2O_3 ceramics with 4 to 6 mol % Y_2O_3 annealed in the two phase (c + t) region for longer periods of time. It was shown that in early stages of annealing a "tweed" structure of t-ZrO_2 was developed. With increasing annealing time this tweed structure becomes coarser and changes into internally twinned "colony" structure. The "colonies" can grow to large sizes but their twin-spacing remains almost constant. The effect of increasing annealing temperature was shown to be more obvious than prolonging annealing time in the transition from tweed to colony structure. The mechanism of the diffusional c–t transformation was discussed.

1. Introduction

Transformation toughening in ZrO_2 based ceramics requires the presence of tetragonal (t) ZrO_2 phase, so that the toughening obtainable from its stress-induced martensitic transformation to monoclinic (m) phase can be realized. ZrO_2 ceramics containing 1.5–3.0 mol % Y_2O_3 fabricated properly to nearly 100% fine-grained t-phase in the structure (TZP) exhibited a very high fracture toughness and strength [1, 2]. On the other hand, in past years ceramists were greatly concerned with the destabilization of c-ZrO_2 and the degradation of mechanical properties caused by the phase transformation above mentioned [3, 4]. Recently, the recognition that t-ZrO_2 could transform from c-ZrO_2 matrix and subsequently undergo the stress-induced martensitic t–m transformation [5, 6] was one of the crucial discoveries leading to a current interest in transformation toughening of ZrO_2 ceramics.

The high ZrO_2 tetragonal distorted-fluorite phase in the ZrO_2–Y_2O_3 system appears to be quite different from those observed in other well-studied partially stabilized zirconia ceramics (Mg–PSZ, Ca–PSZ) [6, 7]. The occurrence of a diffusional c–t transformation during annealing in the c + t two phase region of ZrO_2–Y_2O_3 system was first reported by Heuer *et al.* [3, 8] and then studied by Yagi and his co-workers [9]. Twinned colonies of t-ZrO_2 transformed from the c–ZrO_2 matrix during annealing indicate that various high temperature phase transformations which control the morphology, size and location of t-ZrO_2 phase become very important. This paper focuses on the diffusional c–t phase transformation in ZrO_2–Y_2O_3 ceramics containing 4 to 6 mol % Y_2O_3 annealed in the c + t two phase region for long periods of time. Details of the nature of the microstructural evolution associated with this transformation were discussed.

2. Experimental procedure

Zirconia powders with 4, 5 and 6 mol % Y_2O_3 and average grain size of 0.05–0.1 μm were supplied by Japan Toso Co. The powders were cold isostatically pressed (CIP) at 400 MPa and then sintered in air at 1500–1600 °C for 2 h followed by furnace cooling. The samples were annealed in the temperature range 1100 to 1500 °C for 4 h to 1400 h followed by furnace cooling. The sintering and annealing of the samples are shown in the ZrO_2–Y_2O_3 phase diagram given in Fig. 1. The structural analysis and the determination of lattice parameters were performed by using a Japan Scientific X-Ray Diffractometer. Microstructural observations of thin foils prepared by ion-thinning were carried out in a Hitachi H-800 electron microscope operated at 200 kV. Electron probe microanalysis was made by using a JEOL fx-2000 scanning transmission electron microscope.

3. Results and discussion

3.1. Early stages of the diffusional c–t transformation

Fig. 2 shows the TEM bright field image and the diffraction patterns of [1 1 1], [0 1 1] and [1 1 2] zone axes of the 6 mol % Y_2O_3 specimens sintered at

0022–2461/91 $03.00 + .12

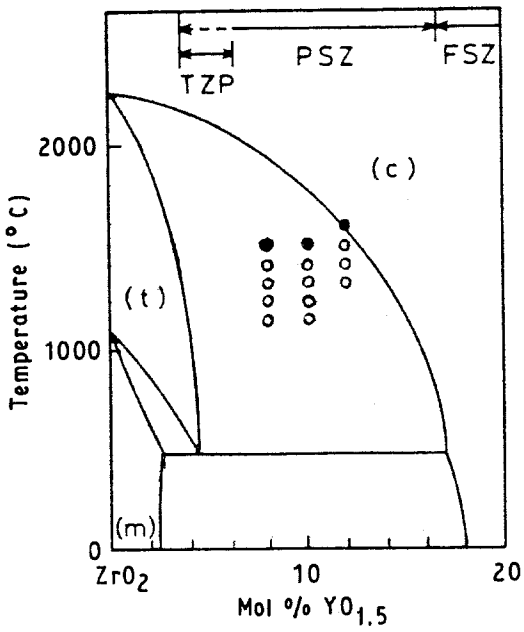

Figure 1 ZrO_2–Y_2O_3 phase diagram showing the composition and the sintering and annealing temperatures of the specimens: (●) sintering, (○) annealing.

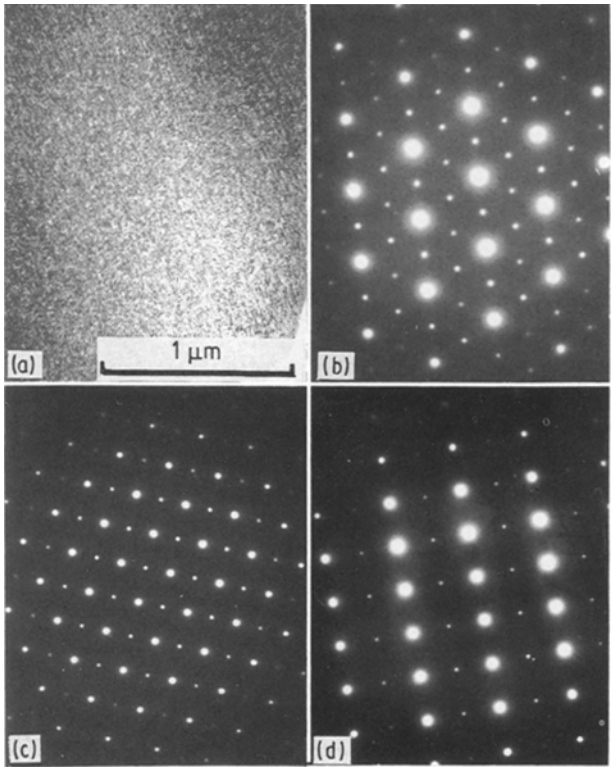

Figure 2 TEM photographs of as-sintered specimens containing 6 mol % Y_2O_3: (a) bring field image; (b), (c), and (d) diffraction patterns of [1 1 1], [0 1 1], [1 1 2], respectively.

1600 °C for 2 h followed by furnace cooling (the asintered state). The features of contrast of the bright field image (Fig. 2a) are very similar to that for the c-phase reported in [10]. However, the diffraction patterns shown in Fig. 2b, c and d indicate the appearance of the three (1 1 2) reflections which are forbidden for the matrix c-phase. This is very similar to the diffraction results of the t′-phase produced from the diffusionless c–t′ transformation [10, 11]. The contrast of very fine and dispersive particles of the second phase may be clearly seen in dark field images taken by three (1 1 2) reflections as shown in Fig. 3. The particles are arranged nearly in two directions with approximately 120° between each other. One can find that every two of the three images are complemental with each other in contrast. XRD analysis of the raw material of ZrO_2 + 6 mol % Y_2O_3 shows a completely cubic structure and this material was sintered at 1600 °C corresponding to the intersecting point of the 1600 °C temperature line with the (t + c)/c phase boundary curve shown in Fig. 1. Therefore, no t-phase will be expected during sintering and the appearance of the (1 1 2) forbidden reflections shows, certainly the presence of t-phase particles formed upon slow cooling from the sintering temperature. The fact that the t-phase of sintered 6 mol % Y_2O_3 specimen was not found in the bright field image (Fig. 2a) but found in dark images only tells that the amount of t-phase transformed only upon furnace cooling from the sintering temperature is rather small so that the pictures shown in Fig. 3 may be considered as characteristic features of the early stages of the diffusional c–t transformation.

Fig. 4 shows the [1 1 1] diffraction pattern and dark field images taken by three (1 1 2) reflections of the 6 mol % Y_2O_3 sample annealed at 1300 °C for 12 h after sintering. Here the sizes of the t-phase particles are coarser and the directionality of their arrangement is clearer in comparison with the photographs shown in Fig. 3 for the as-sintered state. The pictures shown in Fig. 4 may be considered as the medium stage of the "tweed" structure of diffusionally transformed t-phase. When the annealing temperature is increased to 1400 °C, as shown in Fig. 5, the tweed becomes much coarser and the structure seems to be separated into small islands and will be transformed into "colony" structure when the annealing temperature or the annealing time increases further.

3.2. Later stages of the diffusional c–t transformation

The (1 1 1) diffraction pattern and the dark field images taken from three (1 1 2) reflections of the 6 mol % Y_2O_3 specimen annealed at 1500 °C for 12 h are shown in Fig. 6. Typical "colony" structure can be found in Fig. 6b, c and d. In every colony there are black–white internal twins showing different variants of the t-phase. The dark field images (Fig. 6b, c and d) of the colony structure show the same complemental characteristics in contrast as for the case of the tweed structure given in Fig. 3. The results of the electron probe microanalysis of the 5 mol % Y_2O_3 specimen annealed at 1400 °C for 100 h after 1500 °C, 2 h sintering are shown in Fig. 7. It can be seen that the Y_2O_3 content in the colonies is much less than that in the matrix. This can be easily understood if one draws a horizontal line for 1400 °C on the ZrO_2–Y_2O_3 phase diagram (Fig. 1) and the equilibrium Y_2O_3 contents of the t and c phases can be found immediately. XRD analysis shows also the clearly separated diffraction

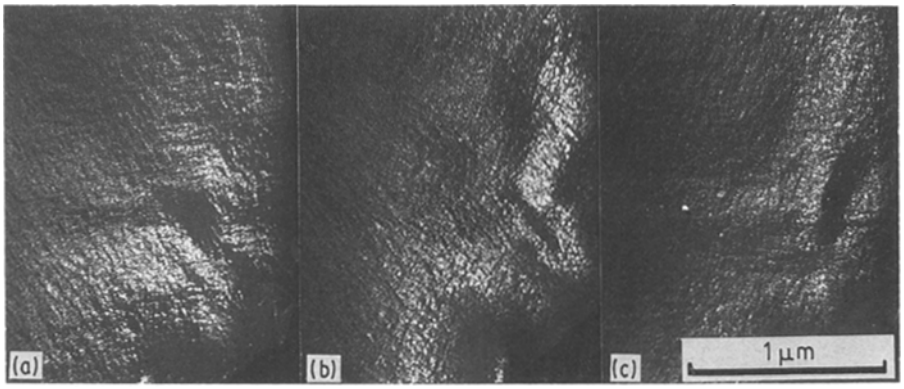

Figure 3 Dark field images of the same area in specimen shown in Fig. 2 taken by three 112 reflections showing the "tweed" structure.

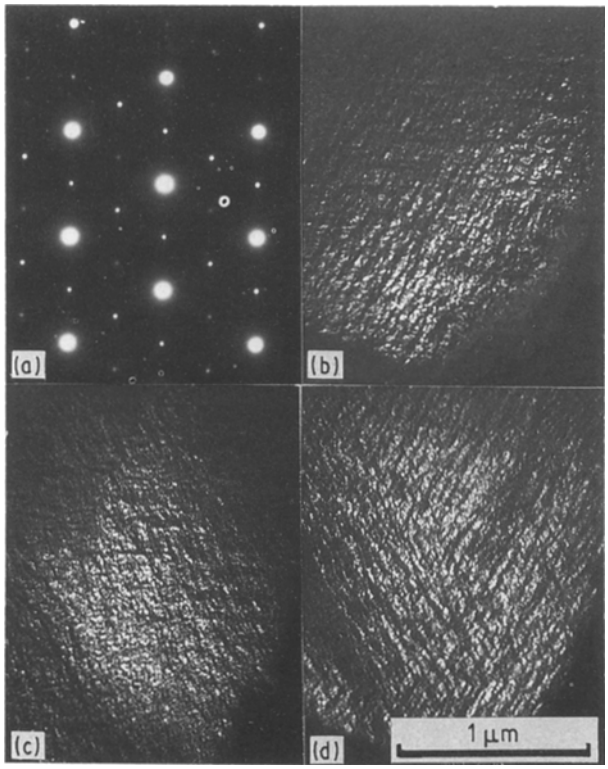

Figure 4 TEM photographs of the 6 mol % Y_2O_3 specimen annealed at 1300 °C for 12 h: (a) a (1 1 1) diffraction pattern, (b), (c) and (d) tweed-like structure in dark field images taken by three (1 1 2) reflections.

peaks of the t-phase together with the peaks of the c-matrix [12].

3.3. Transition from "tweed" to "colony" structure and the growth of "colonies"

It can be seen from Figs 2, 3, 4, 5 and 6 that the tweed and the colony structures are quite different in morphology but identically the same in diffraction patterns. This means that the product t-phase of the diffusional transformation of the c-matrix has the same lattice structure but different morphology depending on the conditions of transformation. Therefore, a continuous transition of the tweed structure to colony structure should be expected. Figure 8 shows the changes of microstructure of the 6 mol % Y_2O_3 specimen annealed from 4 to 16 h at 1400 °C in dark field images taken by (1 1 2) reflections. The 4 h annealed specimen (Fig. 8a) has a typical well developed tweed structure. The 8 h annealed one (Fig. 8b) has a structure mixed by tweeds and colonies. In the 12 h annealed specimen (Fig. 8c) the tweed structure disappeared and the colony structure becomes clearer. And finally, in the 16 h annealed specimen (Fig. 8d), a coarse colony structure formed with no traces of tweeds.

The changes of the size and shape parameters of the colonies with increasing the time for annealing are shown in Fig. 9. It can be seen that width and length of colonies increase monotonically with the annealing time. The number of twin-spacings within a colony increases also with annealing time but the thickness of twin spacings remains constant. This means that the growth of colonies depends mainly on the increase of the number of twin-spacings and the increase of the length of the twins. This is in good agreement with the results of Heuer [13] that the thickness of twin-spacings has reached the equilibrium value at the very beginning of their growth.

3.4. Matrix contrast

Together with the colony structure of transformed t-phase a bright contrast of the c-matrix can also be seen in the dark images taken by (1 1 2) reflections, as shown in Fig. 10, which shows very fine anti-phase domains. This, certainly, is the result of the displacement of oxygen ions indicated by the (1 1 2) reflection [10, 14]. It can be seen from Fig. 10a and b that the contrast of the matrix in the two images are complementary to each other indicating that the complemental areas are variants with different directions of the displacement of oxygen ions. It has been shown in Fig. 10 that during annealing in the two phase c + t range with the transformation of t-phase in colonies the Y_2O_3 content of the matrix becomes larger so that its stability increases and as a result some diffusionless c–t′ transformation can take place upon cooling with the occurrence of t′-ZrO_2 having tetragonal structure but the same chemical composition as the matrix. The size of the antiphase domains is much smaller because of the high Y_2O_3 content in the retained matrix [15].

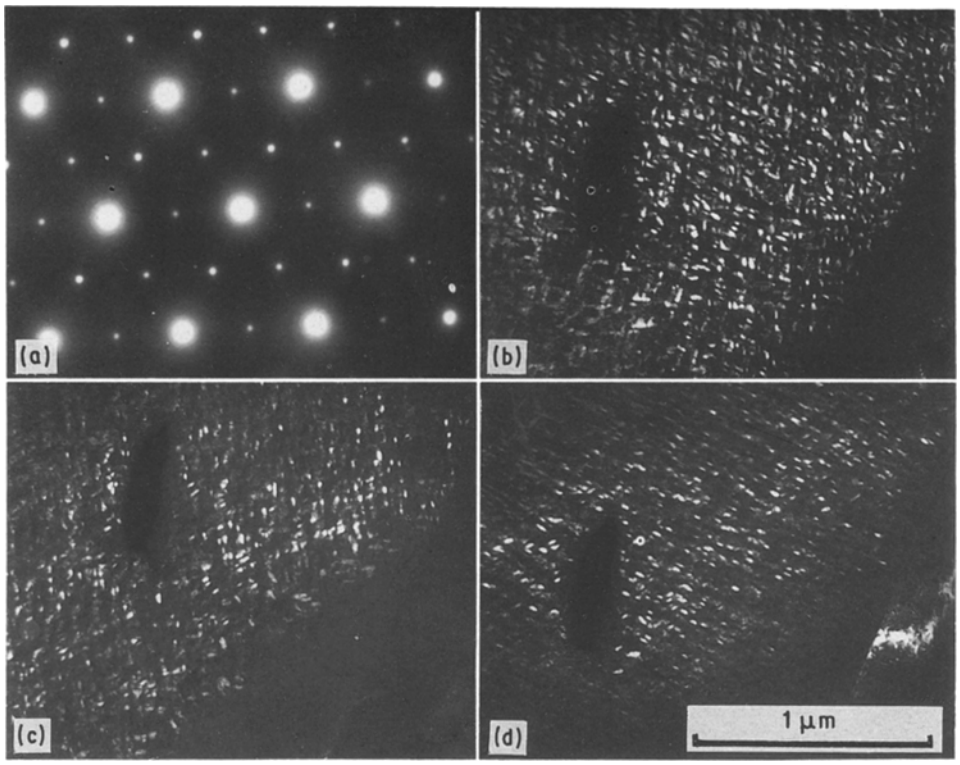

Figure 5 TEM photographs of the 6 mol % Y_2O_3 specimen annealed at 1400 °C for 4 h: (a) a (1 1 1) diffraction pattern, (b), (c) and (d) dark field images taken by three (1 1 2) reflections showing the later stage of tweed structure.

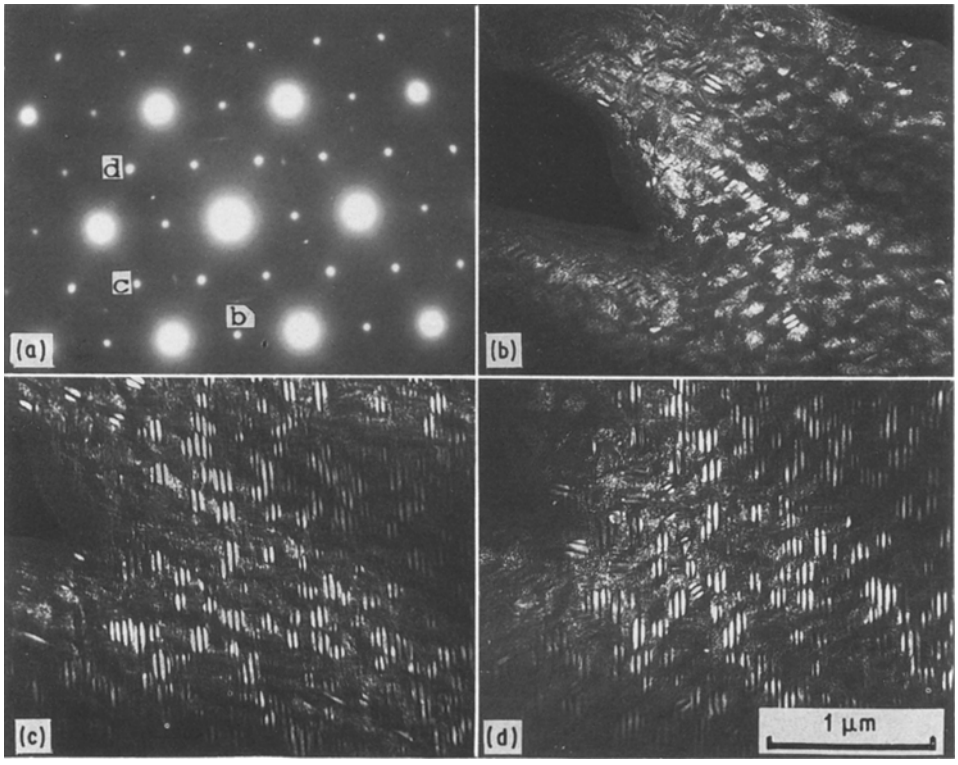

Figure 6 "Colony" structure of the 6 mol % Y_2O_3 specimen annealed at 1500 °C for 12 h: (a) a (1 1 1) diffraction pattern, (b), (c) and (d) dark field images taken by three (1 1 2) reflections.

3.5. Comprehensive diagram of the diffusional c–t transformation

As in cases of the phase transformations in metals, temperature and time are two controlling factors in determining the type and product morphology of transformation. In previous paragraphs the tweed and colony structures have been shown for the ZrO_2 + 6 mol % Y_2O_3 specimen annealed at different temperatures and for different periods of time. Additionally, the structural morphologies of the 5 mol % and 6 mol % Y_2O_3 ceramics annealed at 1200 °C for 1000 h and at 1500 °C for 4 h are shown in Fig. 11. It

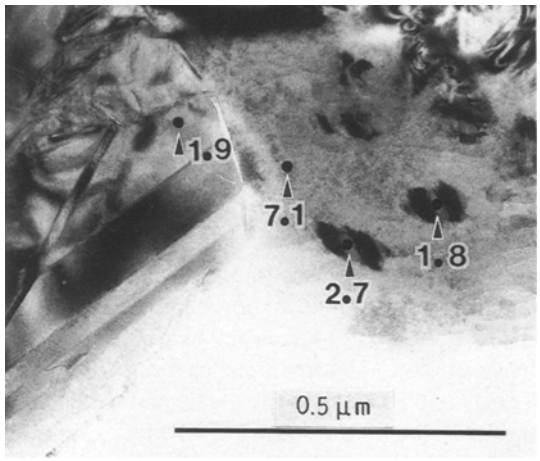

Figure 7 EPMA results of "colony" structure in the 5 mol % Y_2O_3 specimen annealed at 1400 °C for 100 h. The mol % Y_2O_3 content in different areas are shown.

can be seen that in the former case the structure is a typical early-stage tweed one though the annealing time is very long and in the later case there is a well developed colony structure though the annealing time is only 4 h. Therefore, the parameter temperature has much more effect than time in determining the morphology of the product of transformation because the rate of diffusion of atoms is the controlling factor in diffusional phase transformations.

The results of microstructural observations of the ZrO_2–Y_2O_3 specimen with 4 to 6 mol % Y_2O_3 annealed at different temperatures and for different periods of time are summarized in Fig. 12. This is a comprehensive phase transformation diagram like the TTT diagrams for steels. It is quite clear that the tweed structure of transformed t-ZrO_2 appears during annealing at relatively lower temperatures and shorter periods of time while the colony structure appears at higher temperatures and for longer periods of time.

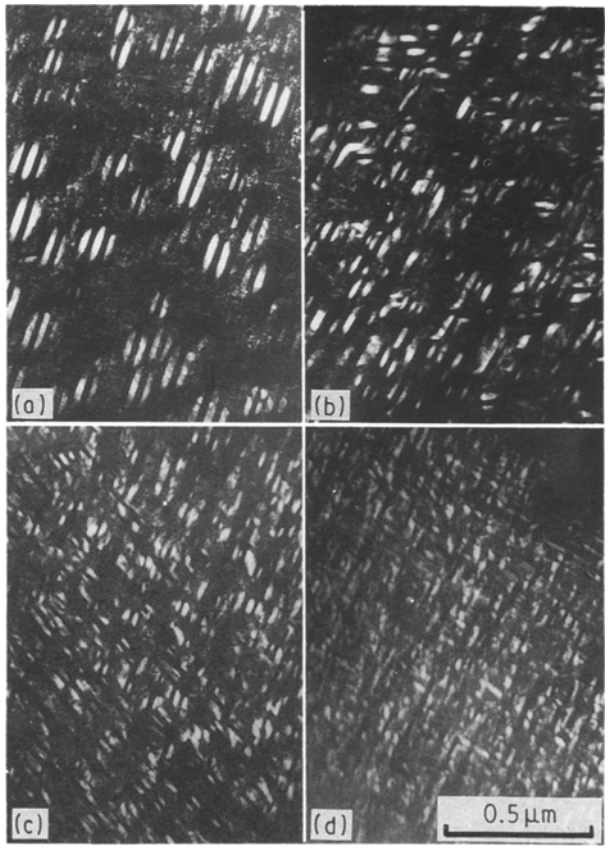

Figure 8 Dark field images taken by (1 1 2) reflections in the 6 mol % Y_2O_3 specimen annealed at 1400 °C for: (a) 16 h, (b) 12 h, (c) 8 h and (d) 4 h.

3.6. Mechanism of diffusional c–t transformation

The cubic to tetragonal phase transformation in ZrO_2–Y_2O_3 ceramics, like transformations in steels, may be divided into two steps: the lattice rearrangement and the adjustment of chemical composition toward the equilibrium state. The lattice rearrangement from cubic to tetragonal structure requires the displacement

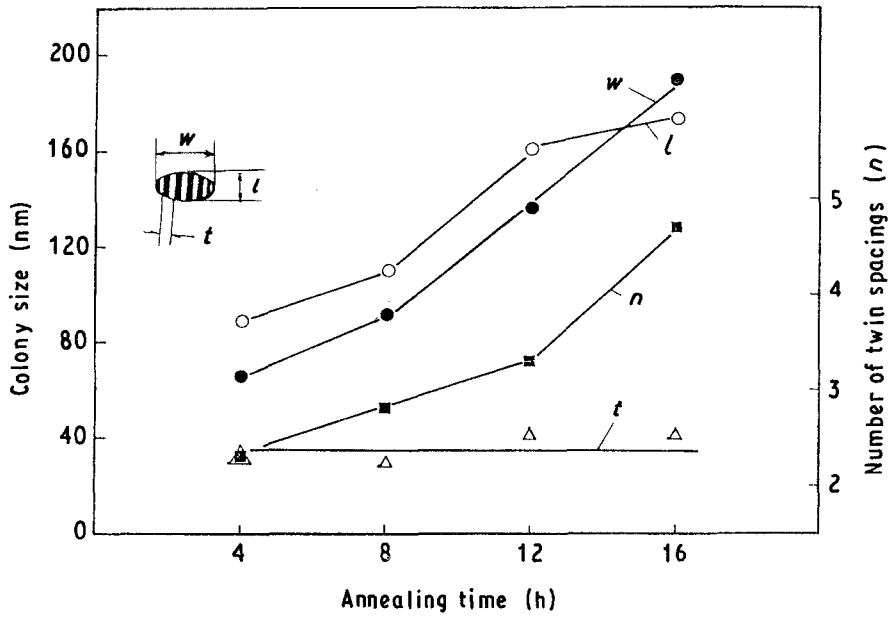

Figure 9 Changes in size and shape parameters of the "colonies" in 6 mol % Y_2O_3 specimen as a function of annealing time at 1500 °C.

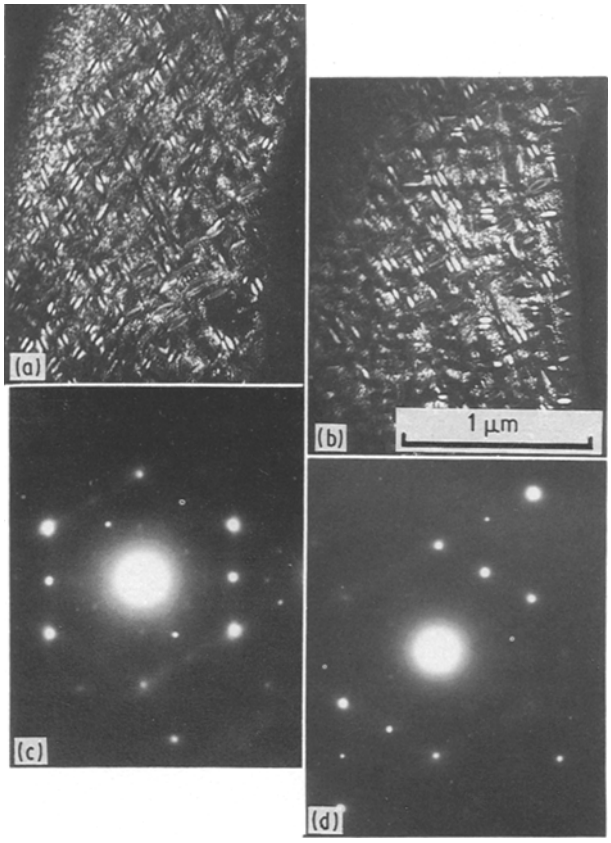

Figure 10 Dark field images (a) and (b) of the 6 mol % Y_2O_3 specimen annealed at 1500 °C for 4 h taken by two (1 1 2) reflections shown in the diffraction patterns (c) and (d) indicating fine domains in the matrix around the colonies.

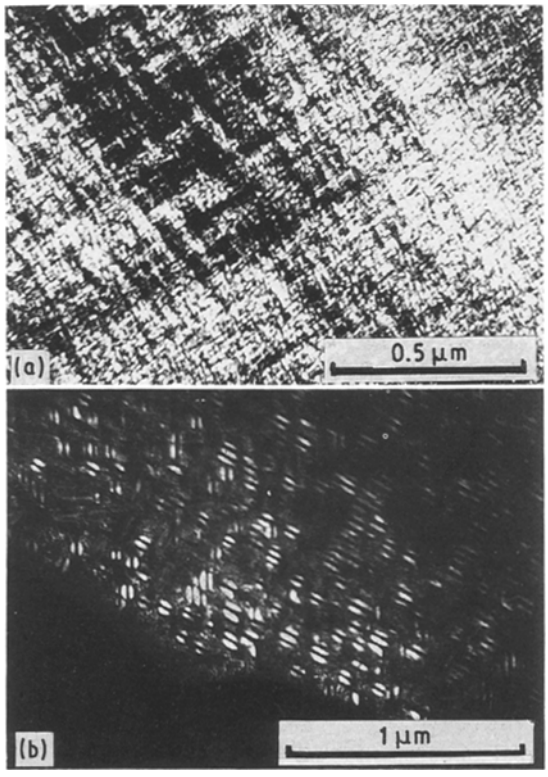

Figure 11 Dark field images taken by (1 1 2) reflections: (a) 5 mol % Y_2O_3 specimen annealed at 1200 °C for 1000 h; (b) 6 mol % Y_2O_3 specimen annealed at 1500 °C for 4 h.

of oxygen ions in order to increase the parameter of the *c*-axis and decrease the parameters of *a*- and *b*-axes. The appearance of tetragonality corresponds to the appearance of (1 1 2) reflections which are forbidden for the cubic phase. In this case a tweed structure forms throughout the specimen and the visible contrast in dark images taken by three 112 reflections is in fact a strain-type contrast induced by the uniformly distributed nuclei of the t-phase. In this moment the chemical composition has not changed yet and remains just as the initial cubic phase. Experimental evidence of this phenomenon has been obtained for the ZrO_2 + 6 mol % Y_2O_3 specimen annealed at 1300 °C for 16 h by the results of EPMA examination:

Point no.	Content of Y_2O_3 (mol %)
1	5.98
2	5.55
3	5.70
4	5.92
5	5.57
6	5.84
7	5.52
8	5.64

This indicates that all tested points have the same chemical composition as in the original state of the specimen. Therefore, no change of chemical composition occurs in the first step of c–t transformation with the appearance of tweed structure.

The second step of c–t transformation requires much longer time for a given annealing temperature because the adjustment of chemical composition from a unique one to two fairly different compositions of the produced t-phase and the retained c-phase according to the ZrO_2–Y_2O_3 phase diagram shown in Fig. 1. The equilibrium chemical composition of the t-phase is much lower in Y_2O_3 content while that of the retained c-phase becomes much higher in Y_2O_3 with comparison with the original specimen. This adjustment of chemical composition requires long distance diffusion of Y and Zr atoms and proceeds parallelly with the microstructural changes from tweed to the colony type. The EPMA data shown in Fig. 7 has already indicated that the colonies of the t-phase have much lower Y_2O_3 content and the retained c-matrix has much higher Y_2O_3 content which are very close to the equilibrium values for the given annealing temperature.

In previous work Sakuma *et al.* [16] have found a structure of spinodal decomposition in arc-melted ZrO_2–Y_2O_3 ceramics with 4 mol % Y_2O_3 annealed at 1700 °C for 10 min. Such spinodal structure may be considered as another type of the tweed structure shown in the present paper. The results of the spinodal structure are also shown in the comprehensive transformation diagram given in Fig. 12.

4. Conclusion

1. The c–t diffusional phase transformation in ZrO_2–Y_2O_3 ceramics can be divided into two steps:

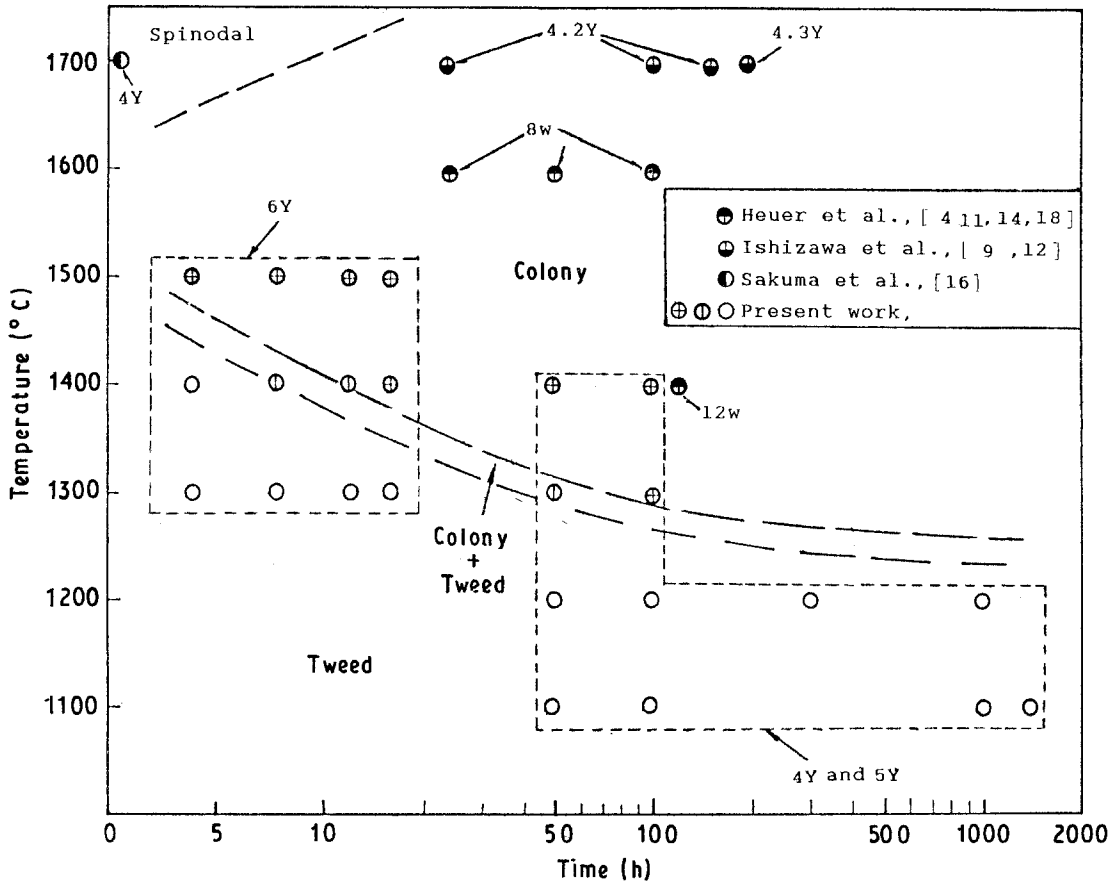

Figure 12 Comprehensive diagram of the diffusional c–t transformation in ZrO_2–Y_2O_3 ceramics. (Y mol % Y_2O_3, W wt % Y_2O_3)

the lattice rearrangement with the appearance of tweed structure and the adjustment of chemical composition with the appearance of colony structure.

2. During annealing at a given temperature the tweed structure gradually changes into the colony structure as the time of annealing increases. The colonies can grow to large sizes but the spacing of their internal twins remains unchanged.

3. The increase in temperature is much more effective than the increase in period of time for the transition from tweed to colony structure during isothermal annealing of ZrO_2–Y_2O_3 ceramics.

References

1. T. SAKUMA, Y. YOSHIZAWA and H. SUTO, *J. Mater. Sci.* **20** (1985) 2399–2470.
2. K. TSUKUMA, Y. KUBOTA and T. TSUKITATE, in "Advances in Ceramics", Vol. 12, Science and Technology of Zirconia II, edited by N. Claussen, M. Rühle and A. H. Heuer (American Ceramic Society, Columbus OH, 1984) pp. 382–90.
3. E. RYSHKEWITH, "Oxide Ceramics" (Academic Press, New York, 1960) p. 350.
4. A. H. HEUER and M. RÜHLE, in "Advances in Ceramics", Vol. 12, *op. cit.* [2], pp. 1–13.
5. C. GAVIE, R. H. HANNINK and R. T. POSCOE, *Nature, Lond.* **258** (5537) (1975) 703–704.
6. D. L. PORTER and A. H. HEUER, *J. Amer. Ceram. Soc.* **62** (1979) 298–305.
7. J. M. MARDER, T. E. MITCHELL and A. H. HEUER, *Acta Metall.* **31** (1983) 387–95.
8. S. C. FARMER, T. E. MITCHELL and A. H. HEUER, in "Advances in Ceramics", Vol. 12, *op. cit.* [2], pp. 152–63.
9. T. YAGI, A. SAIKI, N. ISHIZAWA, N. MIZUTANI and M. KATO, *J. Amer. Ceram. Soc.* **69** (1) (1986) C3 and C4.
10. Y. ZHOU, Ph.D. Thesis, Harbin Institute of Technology, Harbin, People's Republic of China (1989).
11. R. CHAIM, M. RÜHLE and A. H. HEUER, *J. Amer. Ceram. Soc.* **68** (1985) 427–31.
12. N. ISHIZAWA, A. SAIKI, T. YAGI, N. MIZUTANI and M. KATO, *J. Amer. Ceram. Soc.* **69** (2) (1986) C18–C20.
13. A. H. HEUER, R. CHAIM and V. LANTERI, 'Phase Transformation and Microstructural Characterization of Alloys in the Y_2O_3–ZrO_2 System', a review, by private communication.
14. V. LANTERI, R. CHAIM and A. H. HEUER, *J. Amer. Ceram. Soc.* **69** (10) (1986) C258–C261.
15. T. SAKUMA, *J. Mater. Sci.* **22** (1987) 4470–75.
16. T. SAKUMA, Y. YOSHIZAWA and H. SUTO, *ibid.* **21** (1986) 1436–40.
17. H. SCOTT, *ibid.* **10** (1975) 1527–35.
18. V. LANTERI, A. H. HEUER and T. E. MITCHELL, in "Advanced in Ceramics", Vol. 12, *op. cit.* [2], pp. 118–30.

Received 10 May 1990
and accepted 31 January 1991